

# Band Formation during Gaseous Diffusion in Aerogels

M. A. Einarsrud

*Institutt for uorganisk kjemi, Norges teknisk-naturvitenskapelige universitet, N-7034 Trondheim, Norway*

Frank A. Maaø and Alex Hansen

*Institutt for fysikk, Norges teknisk-naturvitenskapelige universitet, N-7034 Trondheim, Norway*

M. Kirkedelen and J. Samseth

*Institutt for energiteknikk, Postboks 40, N-2044 Kjeller, Norway*

(March 23, 2022)

We study experimentally how gaseous HCl and NH<sub>3</sub> diffuse from opposite sides of and react in silica aerogel rods with porosity of 92 % and average pore size of about 50 nm. The reaction leads to solid NH<sub>4</sub>Cl, which is deposited in thin sheet-like structures. We present a numerical study of the phenomenon. Due to the difference in boundary conditions between this system and those usually studied, we find the sheet-like structures in the aerogel to differ significantly from older studies. The influence of random nucleation centers and inhomogeneities in the aerogel is studied numerically.

PACS: 82.20.-w, 82.20.Hf, 82.20.Wt, 05.40.+j

## I. INTRODUCTION

A classic high-school chemistry experiment consists of placing a cotton plug drenched in ammonia at one end of a long glass tube simultaneously with another one drenched in hydrochloric acid at the other end of the tube [1]. Then one waits, and after some time, a white ring forms on the tube wall. The white ring consists of ammonium chloride, resulting from the gases reacting on contact. From measuring the position of the ring relative to the two ends of the tube, the ratio between the average velocities of the two gases is found. This ratio is then compared to Graham's law which states that it is equal to the square root of the inverse of the molar masses of the two gases.

What happens if we repeat this experiment with a porous medium substituting for the air-filled tube? We have performed such experiments, using a silica aerogel as the porous medium. A large number of closely spaced paper-thin sheets form in the aerogel, spanning it in the radial direction. In Figure 1, we show a photograph of the precipitate that was formed by exposing the aerogel rod during 5.5 days to the reacting gases.

Periodic sheet-like structures are known to develop in diffusion-reaction systems. They were first described one hundred and one years ago by Liesegang [2], who observed the reaction when silver nitrate solution diffuses into a gel containing silver dichromate. About a year later, Ostwald [3] suggested that the Liesegang rings are due the presence of a nucleation threshold. The reaction product nucleates only when a threshold concentration is reached. This nucleation depletes the concentration of mobile reaction product in the zone where the concentration is above threshold and its neighborhood, thus stopping the nucleation process here. Meanwhile, the reaction front moves on, building up the concentration of mobile reaction product elsewhere. This leads to the formation of the Liesegang rings. Another theory, put forward by Prager [4], is based on the existence of a reaction threshold between the two diffusing species. An intermediate mobile reaction product is then no longer necessary in order to produce the Liesegang structure, as was the case in the Ostwald theory.

In the subsequent years, hundreds of papers have appeared discussing various aspects of the Liesegang phenomena, including a host of alternative explanations. For reviews see e.g. [5–8]. We note that in standard Liesegang experiments, one of the reactants is already present in the gel at the beginning of the experiment. However, in our experiment the two reactants simultaneously diffuse into the reaction zone.

Usually, the reactants diffuse in an aqueous gel. However, there exist experiments that have demonstrated the Liesegang phenomenon in gaseous systems, notably that of Spotz and Hirschfelder [9] who obtained rings in a tube containing HCl and NH<sub>3</sub>, i.e., the high-school setup described above. As no porous medium was deployed in this study, the reaction product were not kept fixed and the structure of the rings could not be studied.

In the next section we describe the fabrication process of the aerogels used in the experiments and present the results of these. Besides the visual observation of the Liesegang rings, we measure effective diffusion constants and use IR-spectroscopy to more accurately determine the concentration profile of the precipitate. This latter is important since the pore size is about a tenth of the wave length of visible light, making it impossible to assess the true shape of the Liesegang sheets. In section III we present a numerical study of a reaction diffusion system using a slightly

modified Oswald theory resembling the one studied by Dee [10], and with boundary conditions similar to those used in the experiment. The resulting structure of the precipitate is qualitatively very similar to those observed in the experiments. We furthermore study the influence of random nucleation centers and inhomogeneities in the porous medium. Our conclusions are presented in section IV.

## II. EXPERIMENT

### A. Fabrication of aerogel

Silica aerogels are ideal systems to study gaseous diffusion-reaction processes. They are highly porous, with a porosity up to 99.8%. SANS studies [11] reveal a fractal pore structure over a range from 0.5 nm to 50 nm. This is of the order of the molecular mean free path of a gas at standard pressure and temperature. The fractal dimension of the aerogels is in the range of 2.2 to 2.4. At larger scales the gel is uniform. A micrograph presented in [12] shows a gel structure resembling a random fibrous network. The silica aerogels used in the present study were made from tetramethoxysilane (TMOS),  $\text{H}_2\text{O}$ , methanol,  $\text{HCl}$  and  $\text{NH}_4\text{OH}$  in the total molar ratio  $1 : 4.98 : 12.6 : 10^{-3} : 3.810^{-3}$  (for some gels  $1 : 4.98 : 12.6 : 10^{-3} : 1.910^{-3}$ ) following a two-step acid-base catalyzed route described by Brinker *et al.* [13]. To prepare hydrophobic aerogels which were suggested not to chemically interfere with the diffusing gases, the gels were treated with hexamethyldisilazane (HMDZ) in a heptane solution prior to drying. During this treatment a methylation of the gel surface occurs by substituting the OH groups present on the gel surface. The methylation of the gel surface makes it possible to obtain monolithic aerogels at ambient pressure (supercritical conditions are normally necessary) due to a “springback” of the gels during drying [14]. However, from spectroscopic investigations, we note that a small number of remaining OH groups on the pore walls still might act as hydrophilic sites in the system. The bulk density of the aerogels used in this work range from  $0.158 \text{ g/cm}^3$  to  $0.196 \text{ g/cm}^3$ , corresponding to porosities of 92.8% and 91.1%. The aerogels were cast into rods of diameter 8.8 mm, giving an aerogel diameter of about 8 mm. During the diffusion experiments the aerogel rods were covered with a Teflon coating, forcing the diffusing gases to enter the aerogel only through the ends.

### B. Measurements of the effective diffusion coefficients

In order to determine the diffusion coefficients of the two gases  $\text{HCl}$  and  $\text{NH}_3$  in the aerogel, we connected the aerogel rod in series with long glass tube. Cotton plugs drenched in ammonia solution and hydrochloric acid, respectively, were then simultaneously placed at the open ends of the gel rod and the glass tube. By measuring where the  $\text{NH}_4\text{Cl}$  first appears in the glass tube, the diffusion coefficients in the aerogel may be found when the speeds at which the gases move in an air filled glass tube are known. These velocities we determine by placing cotton plugs drenched in ammonia and hydrochloric acid simultaneously in the ends of a long, empty tube — i.e. the high school setup described in the introduction. In the glass tube of length 1.5 m we determine the ratio between the distances from the ends of the tube to the point at which the  $\text{NH}_4\text{Cl}$  precipitate first occurs. We found it to be 2.25.

It should be noted that this result is very different from that predicted by use of Graham’s law, which is 1.47. The reason for this is that chemisorbtion on the surface of the glass tube is important. The precipitate appears after 30 minutes. Thus, combining these two pieces of information, we determine the effective velocities of the two species in the tube to be  $v_{\text{HCl}} = 920 \text{ mm/h}$  and  $v_{\text{NH}_3} = 2070 \text{ mm/h}$ . Our determination of the diffusion coefficients in the aerogels using this method are summarized in Table I. We would have expected samples 1 and 2 to produce equal diffusion constants as the same aerogel is used in these two measurements. The same comment apply to samples 4 and 5. However, they differ by approximately 15%. It is the shorter sample that leads to the smaller diffusion constant for pair 1 and 2, while it is the longer sample in pair 4 and 5 that give the smaller diffusion coefficient. As a result of this lack of systematic trends in the data, we attribute the differences to the accuracy of the method we have used rather than a real effect. We note that the ratio  $D_{\text{NH}_3}/D_{\text{HCl}} = 1.7$  and  $1.5$  based on samples 1 and 3, and 2 and 3 respectively. The ratio between the self diffusion constants of the two gases is equal to the inverse of the square root of their molar masses, i.e. 1.47. That the values we have found in the aerogel are so close to the value predicted by Graham’s law, suggests that the two gases do not interact with the pore walls in a significantly different way. This was expected as we designed our aerogels in order that they should be as chemically inert as possible with respect to the two gases.

We show in figure 2 the result of a two-and-a-half hour diffusion experiment. The precipitate forms a single well-defined narrow sheet. In order to determine whether the precipitation sheet clogs the aerogel, i.e. lowers its permeability significantly, we used the same setup as for the data shown in Table I. An aerogel of length 21.6 mm

was connected to the end of a glass tube of length 1507 mm. Thereafter a cotton plug with ammonia was placed next to end of the aerogel, and a cotton plug with hydrochloric acid was placed at the other end of the glass tube. The position of the first appearance of a precipitate was recorded at a distance 1175 mm from the HCl end, giving a diffusion constant  $D_{NH_3} = 210 \text{ mm}^2/\text{h}$  in the aerogel. The aerogel was then removed, sealed with Teflon tape and cotton plugs drenched in the chemicals were placed at its two open ends. They were left in place for two hours, after which the Teflon tape was removed, and the gel treated in vacuum at 150 C for several hours, thus removing any traces of the diffusing and reacting gases but not the precipitate. The aerogel was then connected to a glass tube of length 1504 mm and a new diffusion-reaction experiment performed. The  $NH_4Cl$  ring now formed at a distance 1182 mm from the HCl end, giving  $D_{NH_3} = 207 \text{ mm}^2/\text{h}$ . Through the Einstein relation, the diffusion coefficient is proportional to the permeability. Thus, with the accuracy of our experimental method, a single precipitation sheet does not influence the overall permeability of the aerogel. We then let a large number of sheets form by continuing the diffusion process over a period of 5.5 days. By repeating the diffusion constant measurements for this system, we detected a relative decrease in the diffusion coefficient of approximately 30%. Thus, there is a detectable influence of the sheets on the permeability.

### C. The Liesegang Sheets

The sheet-like structures we observe in the aerogel system (figure 1) is an example of the Liesegang phenomenon. The sheets are very narrow and span the entire cross section of the aerogel rods. The spacing between the sheets is typically very narrow — often just a fraction of a millimeter. However, much larger gaps occasionally occur in an apparently unsystematic way. We furthermore note that the typical time for the occurrence of the first sheet is a couple of hours, while it takes of the order of a week to generate a pattern such as the one shown in figure 1. We also note that the sheets appear to be only slightly curved, and are surprisingly parallel to each other.

The sheet separation that follow from Ostwald theory in the usual Liesegang setup predicts that the ratio between the position of the rings,  $x_{n+1}/x_n$  approaches a constant  $p$ . This is known as Jablczynski’s law [15]. Furthermore, the ratio between the width  $w_n$  of successive rings,  $w_{n+1}/w_n$  approaches  $p^\alpha$  where  $\alpha = 0.5 - 0.6$  [7]. However, we note that the *boundary* conditions that we employ here differ from those studies where these laws have been found. Thus, we do not expect these to hold in our case. This we find experimentally, and, as we shall see in section III, numerically. We furthermore note that the spatial separation of the sheets increases with decreasing concentration of the reactants. We will discuss this further in the next section.

As the pore size of the aerogel system is of the order of 50 nm or less, i.e. a tenth of the wavelength of visible light, a single pore filled with precipitate is invisible. Thus, in order for the precipitate to be visible, numerous neighboring pores must contain precipitate. This suggests that there is a effective concentration threshold for visibility of the precipitate.

One may then speculate whether the sharpness of the sheets is an optical illusion. In order study this, we measured the concentration of  $NH_4Cl$  in the aerogel using IR spectroscopy. This method consists in removing approximately volumes of one  $\text{mm}^3$  of the areogel from various points in the rod, analysing these separately. In figure 3, we show the result of this study. As is evident, not only is there precipitate outside the sheets, but the concentration of the precipitate is at some points surprisingly high even though no sheet is visible there. Perhaps we are dealing with sheets just below the visibility threshold?

As we will see in section III, the numerical study predicts very sharp sheets. Thus, we may interpret the IR sptroscopy results as evidence of a substructure of sheets below the visibility threshold, rather than few and diffuse sheets.

## III. NUMERICAL SIMULATION

As seen above, the structure of the Liesegang sheets found in the present experiment differs from those resulting from using “traditional” boundary conditions. It is the aim of this section to qualitatively investigate the standard Ostwald theory [10] under the present boundary conditions. Due to the very fast reaction between HCl and  $NH_3$ , we believe that a nucleation threshold for the reaction product, rather than a reaction threshold, as suggested by Prager [4], to be the underlying mechanism.

We start by modeling the system in one dimension. This assumption is justified by the fairly parallel alignment of the observed sheets, and the large aspect ratio of the aerogel rods. We therefore consider the following one-dimensional time-dependent set of equations,

$$\partial_t a(x, t) - D_{NH_3} \partial_x^2 a = -Rab \quad (1)$$

$$\partial_t b(x, t) - D_{HCl} \partial_x^2 b = -Rab \quad (2)$$

$$\partial_t c(x, t) - D_{NH_4Cl} \partial_x^2 c = +Rab - N_1 f(c) c^2 - N_2 cs \quad (3)$$

$$\partial_t s(x, t) = N_1 f(c) c^2 + N_2 cs. \quad (4)$$

The four different functions,  $a, b, c$  and  $NH_4Cl(s)$ , represents the concentration of the reactants  $NH_3$  ( $NH_3$ ) and  $HCl$  ( $HCl$ ),  $NH_4Cl$  in gaseous form ( $NH_4Cl(g)$ ) and lastly  $NH_4Cl$  in solid form ( $NH_4Cl(s)$ ). While the left hand sides of the equations describe the free motion of the species, the right hand sides describe their interactions. The reaction of  $NH_3$  and  $HCl$  into  $NH_4Cl$  is assumed to be fast, i.e.,  $R \gg N_1, N_2$ . The term  $N_1 f(c) c^2$  describes the nucleation of gaseous  $NH_4Cl$  into its solid form, while  $N_2 cs$  describes aggregation of gaseous  $NH_4Cl$  into its solid state. On a microscopic level, the formation of the solid state is a rather complex process. However, as a first approximation we let

$$f(c) = \Theta(c - c_0), \quad (5)$$

where  $\Theta(c - c_0)$  is the unit step function. Thus, no nucleation takes place before the local concentration exceeds  $c_0$ . The numerical calculations reveals that the particular choice of the nucleation term is not very important. However, the existence of a threshold value  $c_0 > 0$  where nucleation starts (or which below nucleation is negligible) is very important.

We assume that the fraction of  $NH_3$  and  $HCl$  that reacts is negligible compared to the total amount of reactants. The concentrations,  $a_0$  and  $b_0$ , of  $NH_3$  and  $HCl$  outside the aerogel, are therefore assumed to be constant. By introducing the dimensionless variable  $\xi = x/L$ , where  $L$  is the length of the aerogel, we normalize the diffusion coefficients to  $D \rightarrow D/L^2$  and let the aerogel be defined in the region where  $\xi \in [0, 1]$ . The reaction front is initially formed at  $\xi_0$ , where

$$\frac{\xi_0}{1 - \xi_0} = \sqrt{\frac{D_{NH_3}}{D_{HCl}}}. \quad (6)$$

The asymptotic position of the reaction front,  $\xi_1$ , is found by equality of the incoming fluxes of  $NH_3$  and  $HCl$ . Under the assumption that the reaction region,  $\delta\xi_f$ , is small ( $\delta\xi_f \ll \xi_1, (1 - \xi_1)$ ),  $\xi_1$  is found as

$$\frac{\xi_1}{1 - \xi_1} = \frac{D_{NH_3} a_0}{D_{HCl} b_0}. \quad (7)$$

For the reaction front to cover some distance, it is assumed that the concentration outside the aerogel of  $HCl$  ( $b_0$ ) is higher than the  $NH_3$  concentration,  $a_0$ . This assumption is based on the observation that the sheets develops in the direction of the  $NH_3$  side. We assume that the  $NH_3$  reservoir is on the left hand side ( $\xi < 0$ ) and that the  $HCl$  reservoir is on the right hand side ( $\xi > 1$ ). We set arbitrarily  $b_0 = 10 \times a_0$  in the following. Furthermore, we set the ratios between the diffusion coefficients to be  $D_{NH_3} : D_{HCl} : D_{NH_4Cl} = 1.5 : 1.0 : 0.8$  in agreement with Table I. Note that  $D_{NH_4Cl}$  has not been measured, and that the value chosen is based on the relative masses of the reactants and their product. Furthermore, we have not taken into account that the diffusion coefficients change as a result of the precipitate clogging the pores of the aerogels. We base this assumption on the small effect found in the experiment — see Sect. II B.

The equations (1) – (4) are solved on a discrete lattice with an explicit method. An explicit method is chosen because of the fast dynamics of the reaction. For the one-dimensional calculations the interval  $[0, 1]$  is divided into 1000 cells. Typically  $10^6$  time steps are necessary to follow the process. For each time step, the calculations are done in two steps. First, changes in concentrations in each cell due the reaction  $NH_3 + HCl \rightarrow NH_4Cl$  is calculated with a following correction due to  $NH_4Cl(g) \rightarrow NH_4Cl(s)$ . Second, diffusion takes place.

By increasing the reservoir concentrations,  $a_0$  and  $b_0$ , by a common scaling factor,  $\gamma$ , one can go from the low density regime where the intersheet distance,  $\Delta\xi$ , is much larger than the width of the sheets, via an intermediate regime to a dense regime where sheets start to overlap. The decrease of intersheet distance with increasing reservoir concentrations can be understood by equaling the production rate,  $Rab(\xi_f)\delta\xi_f$  at the reaction front,  $\xi_f$ , with the flux out of the reaction zone at the nucleation threshold. This flux is approximately  $D_{NH_4Cl}c_0/\Delta\xi$ , which gives

$$\Delta\xi \simeq \frac{D_{NH_4Cl}c_0}{Rab(\xi_f)\delta\xi_f}. \quad (8)$$

The width of the reaction front is  $\delta\xi_f$ , and we have assumed that  $\delta\xi_f \ll \Delta\xi$ . In the derivation of equation (8) it is also assumed that the motion of the reaction front is slow compared to the aggregation rate at the nearest sheet. This

implies that the profile of  $\text{NH}_4\text{Cl(g)}$  from  $\xi_f$  to the nearest sheet is approximately linear. One could imagine that a scaling of the reservoir concentrations,  $\{a_0, b_0\} \rightarrow \{\gamma a_0, \gamma b_0\}$ , would give a corresponding scaling of the production rate,  $Rab(\xi_f)\delta\xi_f \rightarrow \gamma Rab(\xi_f)\delta\xi_f$ . However, a scaling of the reaction rate,  $R \rightarrow \gamma R$ , will decrease both the values of  $ab(\xi_f)$  and  $\delta\xi_f$ . Thus, one cannot expect that  $\Delta\xi \sim \gamma^{-1}$ . Figure 4 shows the dependence of  $\log(\Delta\xi)$  on  $\log(\gamma)$  with the two extreme cases of  $\gamma = 0.125$  and  $\gamma = 4.0$  as illustrations. There seems to be no general power law for the scaling of  $\Delta\xi$  with  $\gamma$ , although in the limit of low concentrations it may look as  $\Delta\xi \sim \gamma^{-1}$ . A linear regression on the data of figure 4 gives a slope of  $0.75 \pm 0.03$ .

It is important to notice that as long as the sheets are well separated, the intersheet distance is not dependent on the details of the aggregation and nucleation mechanisms. Only the nucleation threshold is important. This implies that it is possible to find  $c_0$  with knowledge of  $a_0$ ,  $b_0$ ,  $R$  and the diffusion coefficients.

The dynamics of the model can be understood in the following way. At  $t = 0$   $\text{NH}_3$  and  $\text{HCl}$  starts to diffuse into the aerogel. After some time a reaction front is formed at  $\xi_0$ . The reaction front then starts to move to the left, driven by the concentration differences of  $\text{NH}_3$  and  $\text{HCl}$ . After some time the concentration of  $\text{NH}_4\text{Cl(g)}$  is high enough for it to nucleate into  $\text{NH}_4\text{Cl(s)}$ . As the concentration of the solid increases the aggregation process becomes rapid enough to suppress any further nucleation and the left shoulder of the sheet is formed. As the reaction front moves away from the sheet, the flux of  $\text{NH}_4\text{Cl(g)}$  away from the reaction zone drops (the gradient in  $\text{NH}_4\text{Cl(g)}$  decreases). Eventually, the local concentration of  $\text{NH}_4\text{Cl(g)}$  in the reaction front exceeds  $c_0$  and the formation of a new sheet starts. The formation of a new sheet will stop the growth of the first sheet. This process will then continue until the reaction front reaches its asymptotic position,  $\xi_1$ . Figure 5 shows the typical dependence of the sheet concentrations as a function of time. The figure shows that the birth of a new sheet stops the growth of the previous.

From figure 5 we can see that the time between each new sheet is formed increases. This is closely connected with the motion of the reaction front. A new sheet can not be formed before the reaction front is sufficiently away from the last sheet (as argued above). For a more comprehensive understanding, it would therefore be interesting to examine the time dependence of the reaction front position. It would not be unnatural to assume that the density profiles are linearly dependent on  $\xi$ . This approximation should at least be asymptotically correct when  $t \rightarrow \infty$  and  $R \rightarrow \infty$ . However, assume that the density profiles can be approximated as

$$a(\xi) \simeq a_0 \left( \frac{\xi_f - \xi}{\xi_f} \right)^\alpha \quad (9)$$

$$b(\xi) \simeq b_0 \left( \frac{\xi - \xi_f}{1 - \xi_f} \right)^\alpha. \quad (10)$$

By balancing the incoming fluxes with the change in the total amount of the species  $\text{NH}_3$  and  $\text{HCl}$  we obtain

$$\alpha \frac{D_{\text{NH}_3} a_0}{\xi_f} \Delta t = \frac{a_0}{\alpha + 1} \Delta \xi_f + \Delta R, \quad (11)$$

$$\alpha \frac{D_{\text{HCl}} b_0}{1 - \xi_f} \Delta t = -\frac{b_0}{\alpha + 1} \Delta \xi_f + \Delta R, \quad (12)$$

in the limit when  $\Delta t, \Delta \xi_f \rightarrow 0$ . The amount of  $\text{NH}_3$  and  $\text{HCl}$  that reacts and forms  $\text{NH}_4\text{Cl(g)}$  is  $\Delta R$ . From equations (11) and (12) we find that

$$t + t_0 = \frac{a_0 + b_0}{\alpha(\alpha + 1)(D_{\text{NH}_3} a_0 + D_{\text{HCl}} b_0)} \times \left[ (\xi_1 - 1)(\xi_f + \xi_1 \log(\xi_f - \xi_1)) + \frac{\xi_f^2}{2} \right]. \quad (13)$$

where  $t_0$  is a constant. Thus, the reaction front velocity scales with a factor  $\alpha(\alpha + 1)/2$  compared to the case of linear density profiles. The logarithm appearing in this equation predicts a slowing down of the process which is qualitatively consistent with what is observed experimentally — cf. two hours to produce the first sheet, while of the order of a week is necessary to generate a pattern as shown in figure 1. The solid line in figure 6 shows the numerically obtained reaction front position. The broken line represents equation (13) with  $\alpha = 1.25$  and  $t_0$  given by  $t(\xi_0) - t_0 = 0$ , where  $\xi_0$  is defined by equation (6). It is interesting to note that the reaction front initially moves to the right and then turns to the left. Such effects are discussed in Ref. [16], although under slightly different initial and boundary conditions.

So far the numerical model we have studied has been one dimensional. Will the one-dimensional structure of sheets (peaks) survive in higher dimensions in the presence of disorder, and is it possible to understand the bending of the sheets observed in the experiments? In order to study these questions, we present in the following a study of the two-dimensional version of Eqs. (1) to (4).

Disorder can be caused by local concentration fluctuations of the reacting species and presence of inhomogeneities in structure of the aerogel. Also, inhomogeneities in the initial and boundary conditions, which exist in the experimental situation, may influence the resulting sheet structure.

We consider a system of length 1 and width 0.2 (in units of the physical length,  $L$ ). This we represent as a grid of size  $500 \times 100$ . Each unit cell of this grid corresponds to a square of size  $0.1 \times 0.1 \text{ mm}^2$  in the experiment.

First, consider some fixed nucleation centers in the aerogel, i.e., points where the nucleation threshold,  $c_0$ , is zero. Such points will always influence the resulting pattern, and suppress formation of precipitate in a distance  $\Delta\xi$  from that point. The overall influence would therefore depend on the number density,  $n$ , of such centers. As a general criterion for the overall effect of such points to be small, one should require

$$n(\Delta\xi)^d \ll 1, \quad (14)$$

where  $d$  is the spatial dimension of the system. Figure 7 shows the resulting pattern of precipitate for some values of the number density. The nucleation centers are randomly distributed with uniform density.

It is also interesting to study the effect of density variations of the medium. In particular, since such systematic defects may possibly describe formation of fairly parallel but bent sheets. Indeed, equation (8) gives a clear hint that nonparallel alignment is to be expected if the diffusion coefficient is greater on one side of the system than the other. If density variations are formed during the fabrication of the aerogel, this will result in spatial dependence of the diffusion coefficients in all directions. On the other hand, if inhomogeneous conditions are introduced due to elastic compression and stretching in the longitudinal direction, then only  $D_{xx}$  will be spatially dependent. Assume that the diffusion coefficients are of the form

$$D(x, y) = D_0 [1 + \delta \sin(4\pi x/L_x) \cos(\pi y/L_y)]. \quad (15)$$

Figure 8 (a) shows the resulting pattern due to longitudinal compression and stretching with  $\delta = 0.2$ , while figure 8 (b), (c) and (d) shows the resulting pattern due to density variations when  $\delta = 0.2, 0.1$  and  $0.05$  respectively. The resulting pattern due to longitudinal stretching and compression is as expected, but when  $D_{yy}$  also becomes spatially dependent, the formed pattern deviates significantly from the original even for small values of  $\delta$ .

#### IV. CONCLUSION

We have in this paper studied periodic precipitation in a gaseous reaction-diffusion system where both reactants, HCL and  $\text{NH}_3$ , are diffusing into the porous matrix. This is in contrast to the usual way Liesegang phenomena are studied. The matrix is provided by a silica aerogel with approximately 92% porosity. The reaction product,  $\text{NH}_4\text{Cl}$ , precipitates in sheetlike structures which are surprisingly narrow, densely spaced and parallel to each other. There is no apparent structure as to where the sheets appear. Through numerical simulations based on the nucleation theory of Ostwald [3], we reproduce qualitatively the phenomenon.

We thank E. H. Hauge, P. C. Hemmer, J. S. Høye and K. Sneppen for valuable discussions. Thanks are also due to S. Pedersen for performing the IR measurements, and to E. Nilsen for performing some of the diffusion experiments. F. A. M. acknowledges financial support by the Research Council of Norway (NFR).

- 
- [1] See e.g. S.S. Zumdahl, *Chemical Principles* (D.C. Heath, Lexington, Mass. 1995).
  - [2] R.E. Liesegang, *Naturwiss. Wochenschr.* **11**, 353 (1896).
  - [3] W. Ostwald, *Lehrbuch der Allgemeinen Chemie* (Engelmann, Leipzig, 1897).
  - [4] S. Prager, *J. Chem. Phys.* **25**, 279 (1956).
  - [5] K. H. Stern, *Chem. Rev.* **54**, 79 (1954).
  - [6] J. B. Keller and S. I. Rubinow, *J. Chem. Phys.* **74**, 5000 (1981).
  - [7] B. Chopard, P. Luthi and M. Droz, *J. Stat. Phys.* **76**, 661 (1994).
  - [8] É. Kárpáti-Smidróczki, A. Büki and M. Zrínyi, *Colloid Polym. Sci.* **273**, 857 (1995).
  - [9] E. L. Spotz and J. O. Hirschfelder, *J. Chem. Phys.* **19**, 1215 (1951).
  - [10] G. T. Dee, *Phys. Rev. Lett.* **57**, 275 (1986).
  - [11] R. Vacher, T. Woignier, J. Pelous and E. Courtens, *Phys. Rev. B* **39**, 7384 (1989).

- [12] M. Chan, N. Mulders and J. Reppy, *Physics Today* **49**, Number 8, 30 (1996).  
[13] C. J. Brinker, K. D. Keefer, D. W. Schaefer, R. A. Assink, B. D. Kay, and C. S. Ashley, *J. Non-Cryst. Solids* **63**, 45 (1984).  
[14] R. Deshpande, D. M. Smith, and C. J. Brinker, Patent no. WO 94/25149.  
[15] K. Jableczynski, *Bull. Soc. Chim. France* **33**, 1592 (1923).  
[16] Z. Koza and H. Taitelbaum, *Phys. Rev. E* **54**, R1040 (1996).

TABLE I. Diffusion constants for ammonia and hydrochloric acid in different aerogels. Samples 1, 2 and 3 differ in chemical composition from samples 4 and 5. However, each sample within the two groups, 1, 2 and 3, and 4 and 5, are identical. The fourth column contains the ratio between the distances from the two ends of the glass tube including the length of the aerogel to the point at which the precipitation ring first appeared.

Sample number	Tube length (mm)	Aerogel length (mm)	Ratio $\text{NH}_3/\text{HCl}$	$D_{\text{HCl}}$ ( $\text{mm}^2/\text{h}$ )	$D_{\text{NH}_3}$ ( $\text{mm}^2/\text{h}$ )
1	1505	19.85	0.10	79	135
2	1500	10.30	1.02		118
3	1500	10.35	52.12		
4	1500	20.30	0.17		160
5	1500	13.95	0.87		183

FIG. 1. A 2.1 cm long aerogel rod with diameter 8 mm was wrapped in teflon tape along the long axis. At one end of the rod a cotton plug soaked in HCl was placed. At the other end, a cotton plug soaked in  $\text{NH}_3$  was placed. After 5.5 days, the cotton plugs and teflon tape were removed. A precipitate consisting of  $\text{NH}_4\text{Cl}$  in the form of a series of clearly defined narrow sheets has formed. The ammonia was placed at the left hand side of the rod, while the hydrochloric acid was placed at the other side.

FIG. 2. An aerogel rod after a diffusion experiment lasting two hours and thirty minutes. The narrowness of precipitation region should be noted. The cotton plug containing hydrochloric acid was placed at the left end of the rod, while the cotton plug containing ammonia was placed at the other end.

FIG. 3. Drawing of aerogel indicating where IR spectra have been recorded in order to determine the amount of  $\text{NH}_4\text{Cl}$  present there. The numbers show amount of precipitate relative to a maximum value. It is clear that there is precipitate present also outside the sheets.

FIG. 4. Intersheet distance,  $\Delta\xi$ , as a function of the scaling of boundary conditions,  $\{a_0, b_0\} \rightarrow \{\gamma a_0, \gamma b_0\}$ . The solutions with  $\gamma = 0.125$  and  $\gamma = 4.0$ , corresponding to the two extremes in the data, are displayed at the top.

FIG. 5. Typical time dependence of sheet concentrations. Each curve represents the maximum concentration of  $\text{NH}_4\text{Cl}(\text{s})$  in each sheet.

FIG. 6. Time evolution of the reaction front position. The solid line represents the numerical solution, while the broken line represents Eq. (13) with  $\alpha = 1.25$  (see text).

FIG. 7. Influence of randomly placed nucleation centers: (a)  $n(\Delta\xi)^2 = 0$ , (b)  $n(\Delta\xi)^2 = 0.023$ , (c)  $n(\Delta\xi)^2 = 0.056$  and (d)  $n(\Delta\xi)^2 = 0.23$ .

FIG. 8. Effects of an inhomogeneous medium: (a); longitudinal compression and stretching,  $\delta = 0.2$ . (b), (c) and (d); density variations,  $\delta = 0.2, 0.1$  and  $0.05$  respectively.

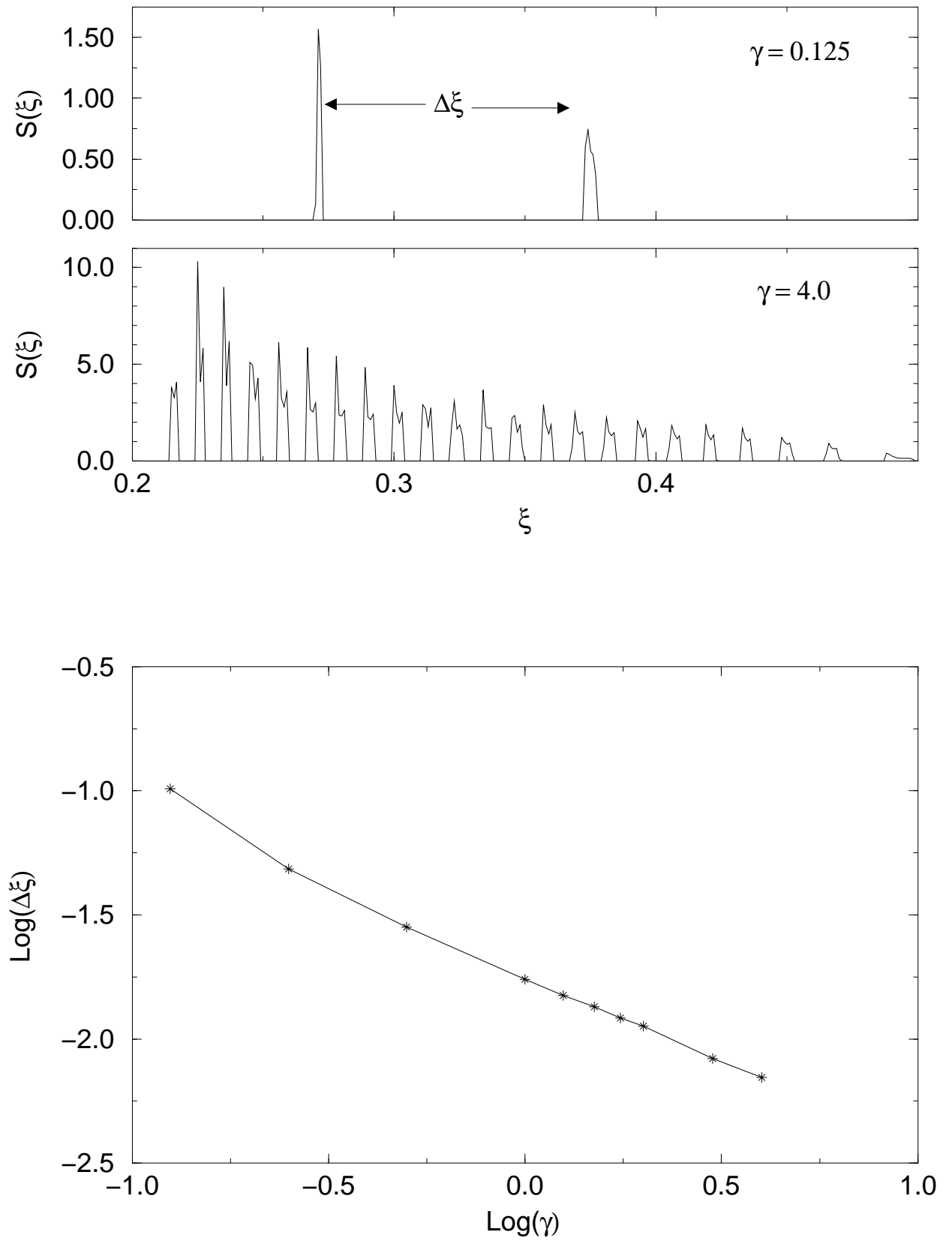


FIG. 4. “Band Formation in ...”: M. A. Einarsrud et al.



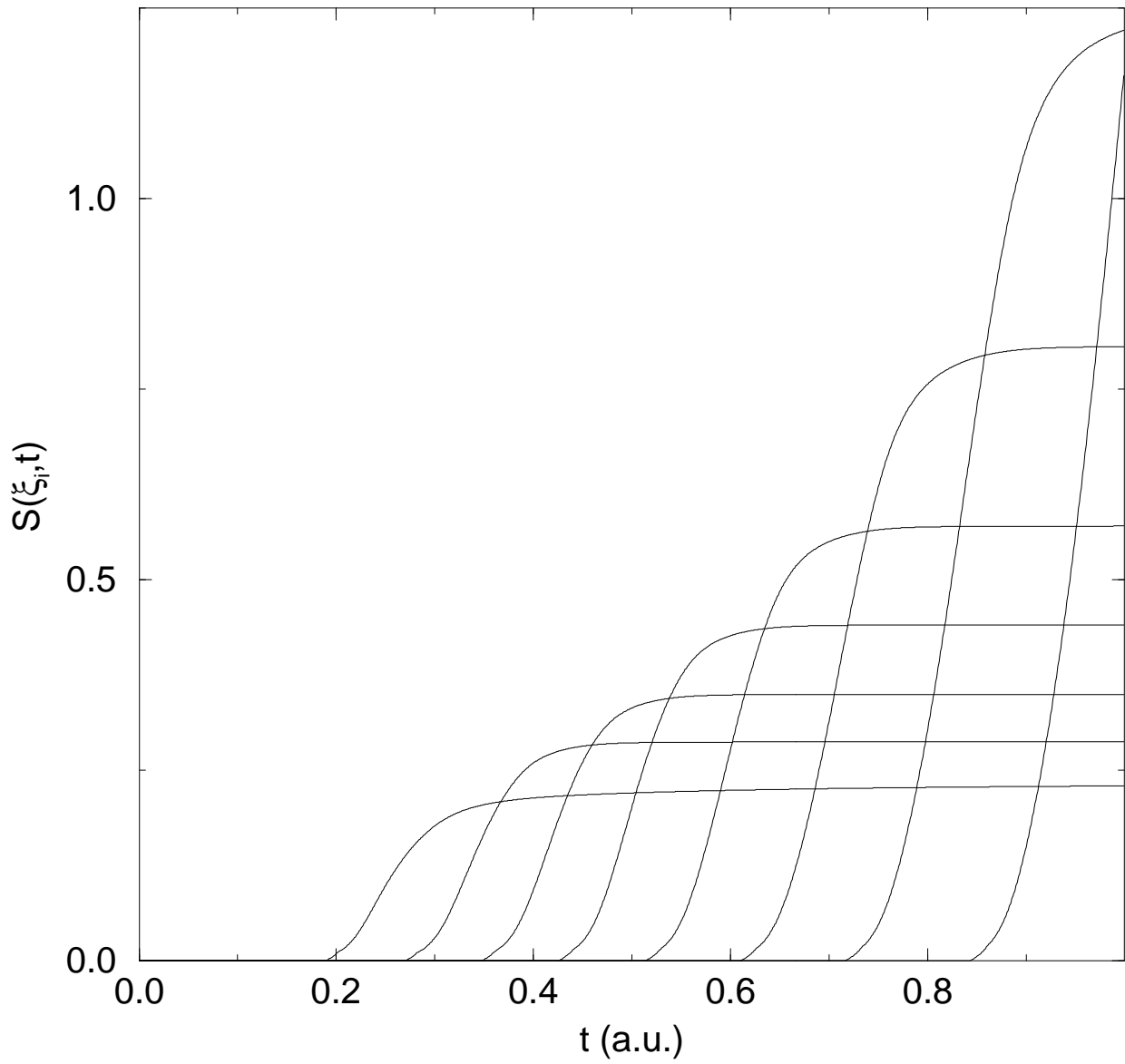


FIG. 5. “Band Formation in ...”: M. A. Einarsrud et al.

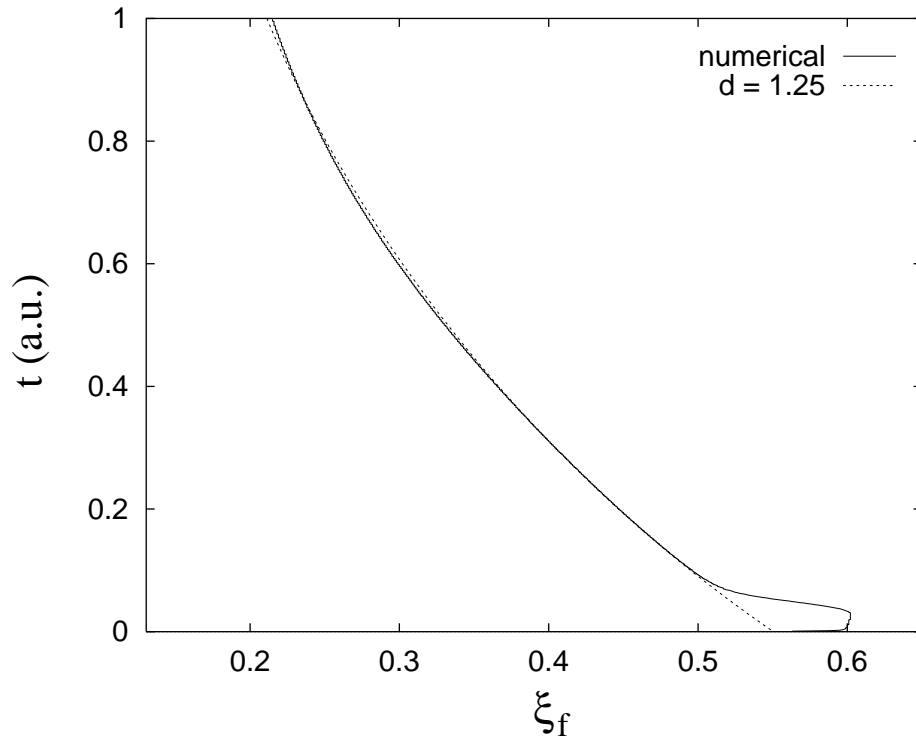


FIG. 6. “Band Formation in ...”: M. A. Einarsrud et al.

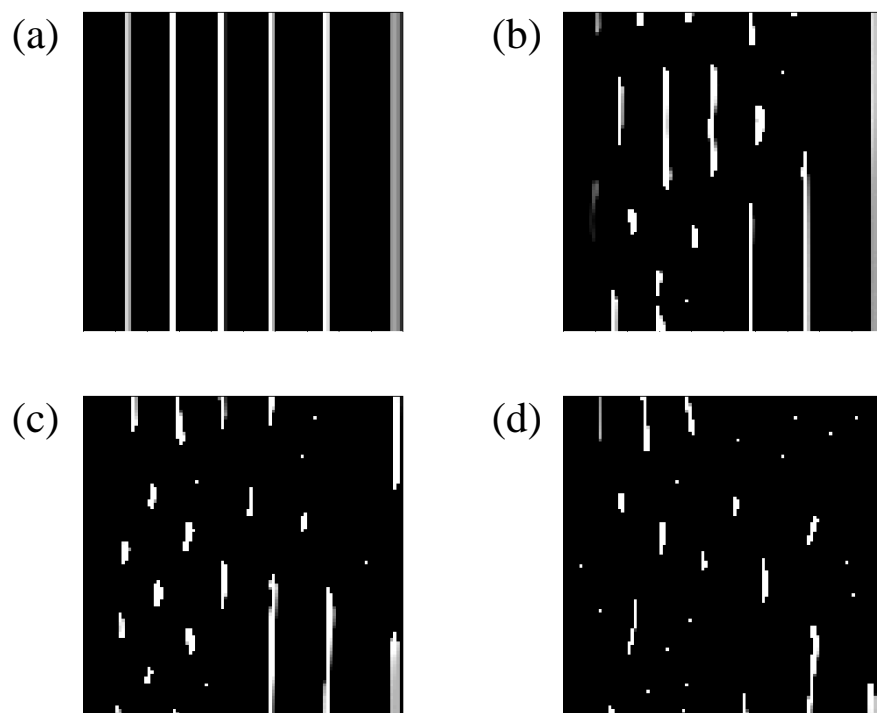


FIG. 7. “Band Formation in ...”: M. A. Einarsrud et al.

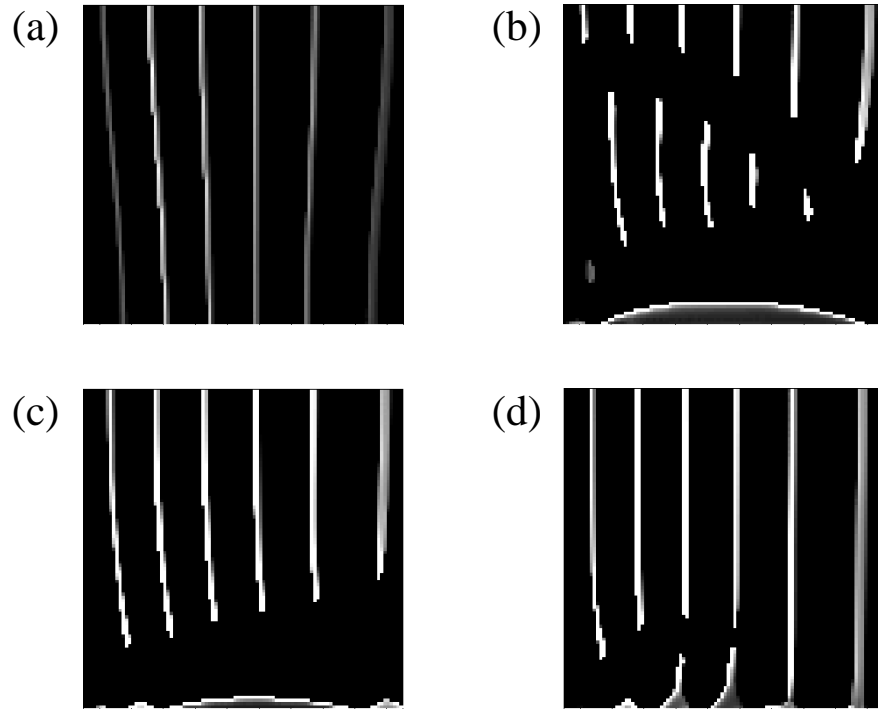


FIG. 8. “Band Formation in ...”: M. A. Einarsrud et al.